Tribology in Full View

Laurence D. Marks, Oden L. Warren, Andrew M. Minor, and Arno P. Merkle

Abstract

For many years, a fundamental problem in contact mechanics, both tribology and indentation problems, has been the inability to see what is taking place—the buried-interface problem. Over the past few years, there have been developments whereby it has become possible to perform contact mechanics experiments *in situ* within a transmission electron microscope. These new experiments have been enabled by both the miniaturization of sensors and actuators and improvements in their mechanical stability and force sensitivity. New information is now becoming available about the nanoscale processes of sliding, wear, and tribochemical reactions, as well as microstructural evolution during nanoindentation such as dislocation bursts and phase transformations. This article provides an overview of some of these developments, in terms of both the advances in technical instrumentation and some of the novel scientific insights.

Introduction

A fundamental aspect of tribology is the modification of the nanoscale structure at the sliding interface, in terms of both mechanical changes during sliding and the consequences of what is, in effect, nanoindentation. As illustrated in Figure 1, a sliding interface includes both regions where there is sliding (S) and regions where there is nanoindentation (N). Experiments in tribology have long suffered from the inability to directly observe what takes place at this sliding contact—the classic buried-interface problem. Sliding interfaces have been studied in a detailed manner by scanning probe microscopy,[1,2] quartz crystal microbalance,[3,4] and surface-force apparatus techniques.[5] In addition, a number of techniques have been developed that can obtain some *in situ* information such as optical spectroscopies[6–9] and x-ray photoelectron spectroscopy.[10] In a few cases, dynamic processes at monolayer interfaces have been observed, for instance, motion of misfit dislocations[11] (i.e., dislocations present to account for the different lattices across an interface). Although these methods have identified many friction phenomena on the nanoscale, interpretation issues can arise because of the indirect or *ex situ* characterization of the contact surfaces or because the techniques are performing volume-averaged measurements, rather than giving direct insight into what is taking place at a single asperity–asperity contact.

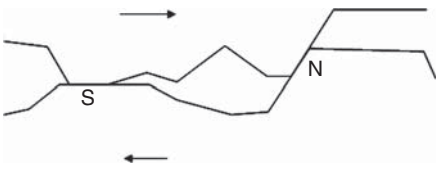

Figure 1. Schematic of a sliding interface showing regions where there are both sliding contact (S) and nanoindentation (N).

To put this difficulty into context, consider that many of the main processes associated with mechanical deformation of materials have been revealed by transmission electron microscopy, either by *in situ* examination or by examination of representative regions postmortem. Unless the two materials have, in effect, welded together (which, for friction, is typically the least desirable of all processes), preserving the interfacial structure so that it can be examined later is exceedingly difficult. Much more common is to separate the two sliding pieces and then perform a retroactive analysis of the transfer layer (material transferred from one surface to another) or examine the wear debris to try to reconstruct the wear events. Although such an analysis has certainly led to enormous improvements in our scientific understanding, at the same time, one always has to worry that the interfacial region might have changed or that the models of the underlying processes that one generates from retroactive analysis might not be fully correct.

An ideal experiment would be to slide a single asperity against a surface, image the event in real time at the atomic scale at both the structural and chemical levels, and correlate this information with all of the applied forces and surface tractions of the system. Although such an experiment cannot yet be performed in detail, it can be approached by the use of transmission electron microscope (TEM) holders (typically rod-like insertion devices for holding a sample under the electron beam) designed principally for scanning tunneling microscopy, atomic force microscopy, or nanoindentation. In common to these *in situ* holders is the ability to finely manipulate the relative position of a sharp tip and, optimally, an electron transparent sample, usually in all three spatial dimensions, which enables them to perform *in situ* contact probing.

In Situ Contact Probes

The use of *in situ* contact probes in TEMs has a surprisingly long history, but the progress made over the years has been sporadic, mostly because of the numerous challenges presented by these instruments. For instance, the high-vacuum environment leads to very high mechanical quality factors (i.e., the sharpness of the mechanical resonance peak, which is larger in vacuum than in air) and restricts the choice of construction materials; the high-energy electron beam can cause charging unless a pathway for charge dissipation is provided; and the very strong magnetic field excludes certain actuation and sensing strategies and further restricts the choice of construction materials. In addition, other issues arise related to unconventional device/sample alignment, in particular, problems potentially caused by the indentation axis being perpendicular to gravity. Most importantly, very limited space is afforded by TEM holders and the sample environment. The cross-sectional diameter of the inserted rod ranges from ~10 mm to ~3 mm, and the thickness of the tip end of the holder can be restricted to less than 2 mm depending on the pole-piece design and the desired range of sample tilt. Therefore, the history of *in situ* contact-probe measurements is as much about impressive achievements in device miniaturization as it is about scientific investigation; compromises in performance versus space are inevitable.

Designs for *in situ* contact probes in TEMs have been published as far back as 1970. In a remarkable, though now largely

forgotten publication, Gane[12] reported an *in situ* contact probe designed specifically for the AEI Scientific Instruments E.M. 6 TEM instrument, which followed other designs by Gane[12] and Gane and Bowden[13] for the scanning electron microscope. The piezo bimorph actuator (i.e., one that bends up and down with applied voltage) shown in Figure 2 was the critical device. Although the method of force determination was not described, the piezo bimorph was reportedly capable of applying loads in the range from 2 μN to 10 mN. However, the environment, probably the lack of damping by air molecules as well as acoustic noise, was found to be detrimental to mechanical vibrations, and a silicone oil dashpot (conceptually similar to an automotive shock absorber, not shown in Figure 2) was incorporated to dampen the tip vibration amplitude to ~5 nm. Using this apparatus, small volumes of materials were stressed in various ways, such as indenting soft materials with hard tips, blunting soft tips against hard countersurfaces, compressing soft spheres between two hard platens, and bending wires. These experiments were performed discontinuously; that is, still photographs were taken after each load increment. Judging from its overall shape, the piezo-bimorph-based apparatus must have been built into the TEM column rather than incorporated into a TEM holder.

The major step forward did not occur until the late 1980s with the work of Spence et al.,[14–17] who fabricated a scanning tunneling microscope within a TEM, which was fairly rapidly followed by home-built instruments[18–26] capable of moving the tip at high resolutions within the instrument while operating in the transmission mode, by the use of either a piezoelectric actuator or an electrostatic comb drive. Coarse positioner design is actually more difficult than fine positioner design, and various schemes have been tried, such as the compact three-dimensional inertial slider mechanism developed by Svensson et al.[26] In recent years, in relationship to *in situ* atomic force microscopy or *in situ* nanoindentation, a number of spring-based devices have been implemented in TEM holders for quantitative force sensing or generation with sub-micronewton sensitivity,[27–37] some relying on the TEM itself to detect the amount of spring deflection (e.g., that of a cantilever with known stiffness) and others determining the force directly through capacitive, piezoresistive, or optical lever sensing or by calibrated electrostatic actuation. These *in situ* contact probes are all of the side-entry type, and continuous recording of real-time images of the evolving tip–sample interaction could now be done. With enough design attention to mechanical vibration suppression, it is possible to resolve atom columns during *in situ* contact experiments.[21–23]

Over the past few years, it has become much easier to exploit the type of instrumentation developed for scanning probe microscopy or nanoindentation within a TEM. With the advent of several commercial systems from Hysitron and Nanofactory, among others, such experiments can now be performed at much higher resolution and imaged in real time. Although an *in situ* contact probe with three axes of quantitative force determination remains elusive, one shouldn't lose sight that much can be done in *in situ* tribology using the existing technologies. In current configurations, one typically uses a small tip, either a scanning tunneling microscopy/atomic force microscopy tip or one designed for mechanical stability in the case of nanoindentation experiments, that can be slid against or indented into the sample, as sketched in Figure 3.

In Situ Observations of Sliding Contacts

The simplest illustration of nanoscale processes taking place during sliding contact is plowing deformation, a common explanation for high friction and wear rates between metals. Figure 4 shows a series of still bright-field images from a television-rate video capture of a gold film being deformed.[38] As the slider passes across the sample, a gouged track is left plastically deformed, providing a direct demonstration of plowing on the nanoscale viewed by *in situ* TEM.

A related process that can also lead to high static friction between metallic surfaces is gouging wear. An example of this type of wear examined *in situ*[38] is shown in Figures 5 and 6. Figure 5 shows part of an indentation series over the course of

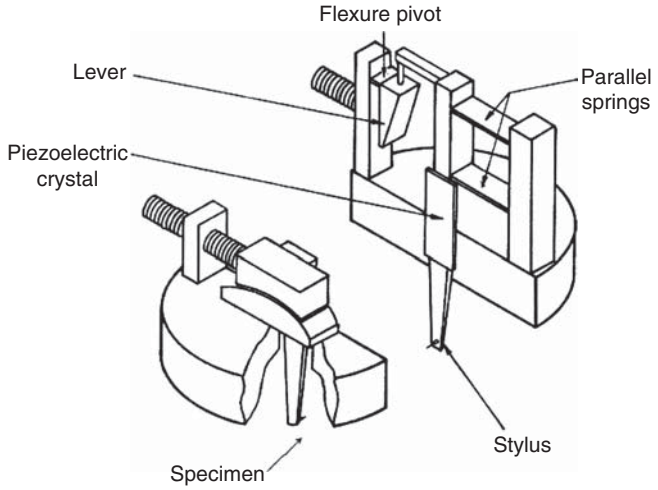

Figure 2. *In situ* contact probe for the AEI Scientific Instruments E.M. 6 TEM instrument. The piezo bimorph actuator ("piezoelectric crystal") is the critical device.

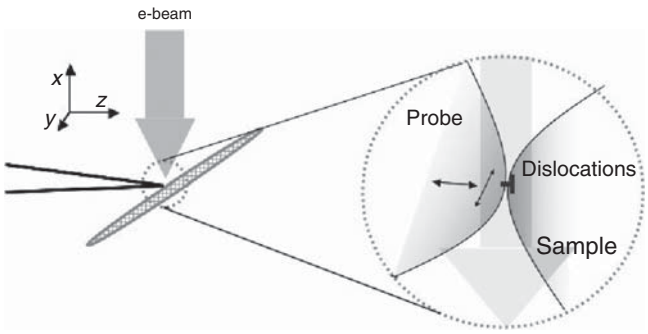

Figure 3. Schematic showing the sliding conditions and imaging geometries used to perform friction experiments within a transmission electron microscope column.

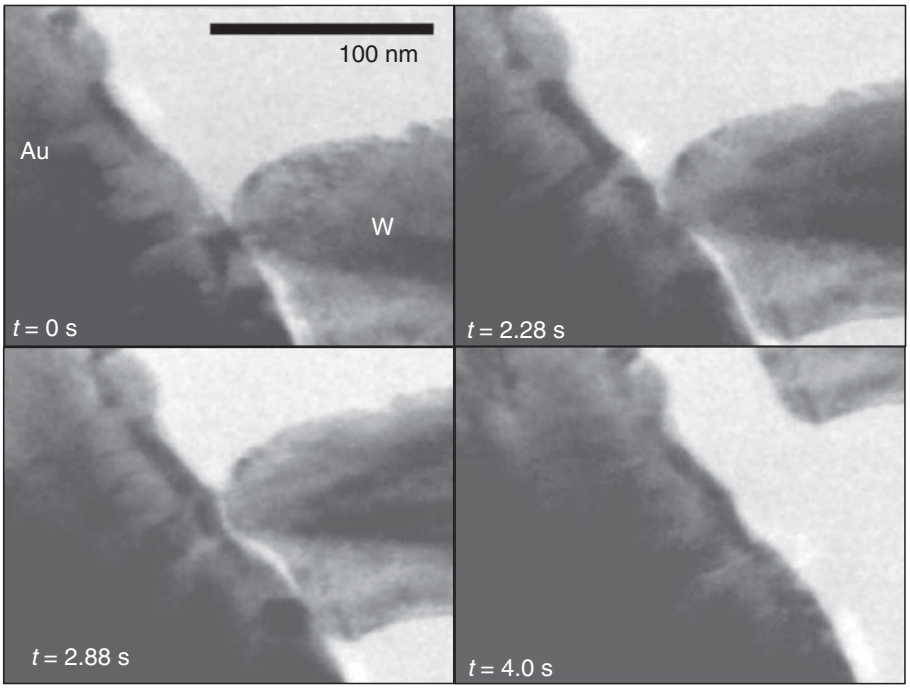

Figure 4. Video stills showing evidence of plowing wear between a tungsten asperity and a gold sample.

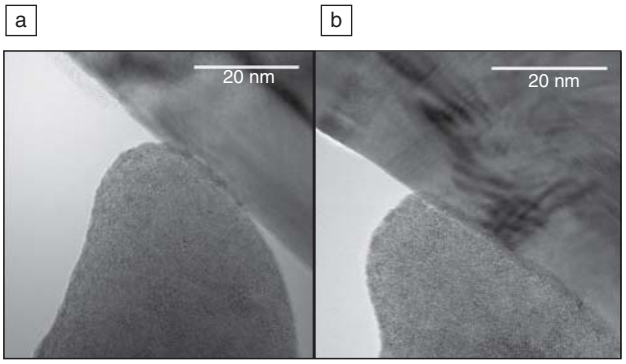

Figure 5. High-resolution transmission electron microscope images of (a) a tungsten probe contacting a Au(110) film and (b) the same system upon application of a larger normal force over tens of minutes. Subsurface deformations are clearly observed during indentation or sliding.

tens of minutes. Bend contours, some periodic, are observed in the gold sample as the harder tungsten tip is pressed against it. Figure 5a shows the initial contact, and Figure 5b shows the sample after the load has been increased. In the latter case, both the probe and sample are bent to a large degree, exhibiting increased bend contour motion in the sample, with little or no observable local plastic deformation by indentation of the tip. When the tip was moved laterally (parallel to the sample edge) to induce sliding, the interface suddenly ruptured, removing a 50 nm × 15 nm piece of the gold film, which remained strongly attached to the tip (Figure 6).

Although gouging wear is common for metallic surfaces, transfer layers (i.e., material transferred from one of the sliding faces to the other) and wear debris are more commonly observed, particularly when one of the materials is known to be a good solid lubricant, such as graphite. During *in situ* sliding of a tungsten tip on graphite, both wear debris and transfer layers have been observed,[39] as shown in Figure 7. Immediately after sliding, the

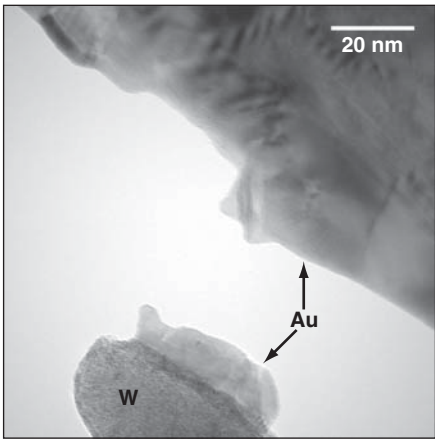

Figure 6. Gold is removed by the tungsten probe sliding parallel to the sample edge after making contact as shown in Figure 5.

tungsten probe was imaged, and transfer of graphitic material to the probe was evident (see Figure 7c), as predicted by Dienwiebel et al.[40,41] in their demonstration of extremely low friction forces. A highly slippery condition arises when a graphite flake attaches itself to the asperity (probe) and forms a graphite–graphite sliding interface.

For the same experiment in the wear region, ordered graphitic wear material was observed, with thicknesses in the range of 5–35 basal plane spacings (2–10 nm) (Figure 7b). The defect structure at a crystalline interface can have an even more direct role in determining friction properties, as it is the motion of dislocations throughout a material, be it at an interface or in the bulk, that is the principal mechanism for deformation in materials. For heterogeneous interfaces consisting of two materials with differing shear moduli, interfacial dislocations will be displaced by some standoff distance into the softer material. The standoff distance for a tungsten–graphite interface can be estimated as 15 nm (44 graphite layers). This estimate is consistent with the thickness of wear flakes observed by *in situ* TEM. Once a graphite flake has been worn and attached to the tungsten probe, the graphite–graphite interface will exhibit no significant dislocation standoff, as the sliding interface becomes the dislocation plane. One can then model the variations in friction as a function of angle[42,43] in terms of the sliding of a graphite rotational grain boundary, where the dominant term turns out to be the density of dislocations: the more dislocations, the easier the sliding.[42,43]

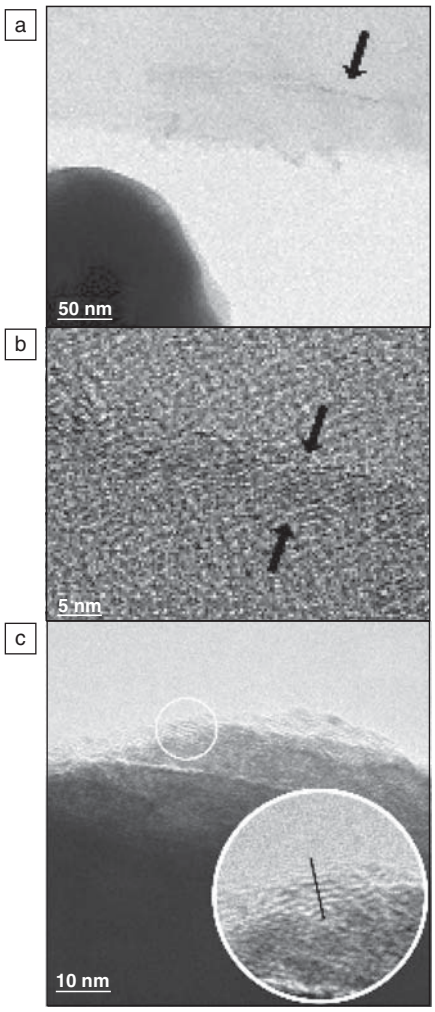

Figure 7. *In situ* transmission electron microscopy evidence of (a,b) graphitic wear by flaking and (c) transfer of graphitic material to the sliding tungsten probe, as evidenced by the 0.34-nm spacings in the circled and enlarged region.

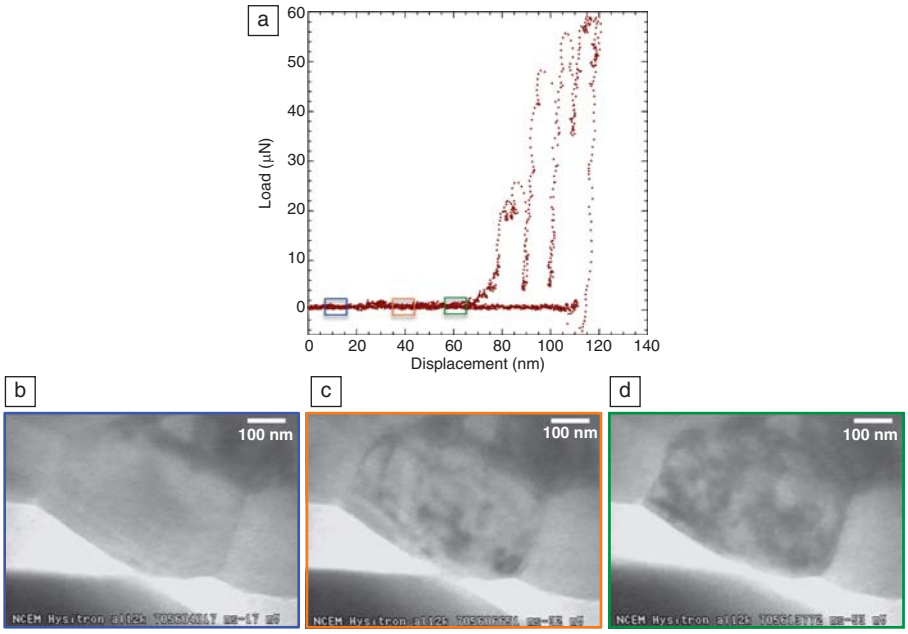

Figure 8. Quantitative *in situ* transmission electron microscope (TEM) nanoindentation of an initially dislocation-free submicron Al grain using a Berkovich conductive diamond indenter. (Adapted from Reference 45.) (a) Displacement-controlled force–displacement curve; and (b–d) video frames of bright-field TEM images showing the microstructure of the studied grain before the first small force transient (blue frame), after the first small force transient (orange frame), and after the second small force transient (green frame). (b) to (c) shows the microstructure change resulting from the first dislocation burst. (c) to (d) shows the microstructure change resulting from the second dislocation burst. Note that the dislocation bursts in b–d occurred before the sustained contact that is denoted by the large increase in load in (a) beginning around 70 nm of displacement.

In Situ Observations of Nanoindentation

Although sliding is one important process taking place, local nanoindentation also occurs as asperities move across the surface. Studies of nanoindentation (and of nanocompression) provide a rich literature of nanoscale deformation processes that are directly relevant to tribology; see, for example, References 12, 13, 33–35, 37, and 44–54. For instance, a recent study of *in situ* nanoindentation of Al thin films[45] demonstrated that permanent deformation below the surface can take place well before the initiation of sustained contact. In Figure 8, an initially dislocation-free submicron Al grain, indented under displacement control, experiences two barely discernible dislocation burst events (barely discernible according to the force versus displacement curve but easily observed in the time-correlated TEM video) well before the start of the apparent initial elastic loading regime. Moreover, the stress that caused the first large load-drop event is near the theoretical level, revealing that a very high stress initiating the first large deformation transient does not necessarily correspond to the onset of plasticity in a dislocation-free volume. The indented grain's dislocation density has already reached a quite high value of ~$10^{14}/m^2$ prior to the first large load-drop event, which is likely the manifestation of grain-boundary confinement of the dislocations. The high dislocation density and a severely locked dislocation structure, evident in the stream of TEM images, might explain the surprisingly high stress. This high-strength mechanism is contrary to the conventional wisdom in the nanoindentation community that theoretical stress just before the point of first obvious yield is indicative of dislocation nucleation in a "perfect" lattice, a notion that has been previously questioned but without the support of *in situ* evidence.[54]

The influence of adhesion on low-force nanoindentation is also relevant to tribology on account of adhesion's contribution to friction. In the same *in situ* study of Al, it was found that dislocation nucleation can occur in an initially dislocation-free grain even when the early-stage tip–sample interaction repeatedly swings between net repulsive and net attractive forces but trends overall into the net attractive force regime (Figure 9). Progressive cracking/destruction of the native oxide, thereby creating increasingly more fresh, sticky Al surfaces, could be the root cause of this behavior. The repulsive/attractive force swings are observed only during tip–sample approach (not during tip–sample withdrawal), so they are unlikely to be a measurement artifact.

In situ nanoindentation results such as these demonstrate the importance of being able to examine subsurface deformation phenomena and provide a sense of the improvement in force sensitivity needed to explore contact phenomena, including tribological phenomena, at an even finer level of detail.

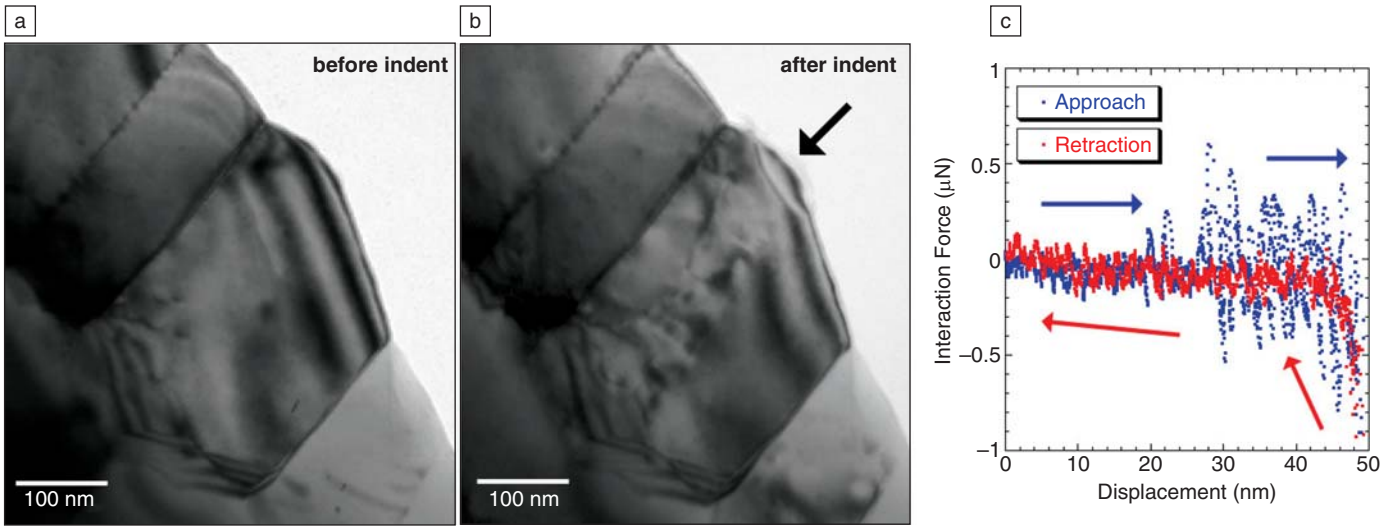

Figure 9. Quantitative *in situ* transmission electron microscope (TEM) nanoindentation of an initially dislocation-free submicron of Al. (Adapted from Reference 45.) (a) Pre-indent bright-field TEM image of the studied grain. (b) Post-indent bright-field TEM image of the studied grain showing the presence of dislocations punched into the grain; the arrow points to the test location. (c) Approach (blue) and withdrawal (red) segments of the corresponding displacement-controlled force–displacement curve.

What Does the Future Hold?

The application of electron microscopy to *in situ* tribology is still in its early stages, and much work remains to be done. From a technical viewpoint, the current instrumentation is not ideal; for instance, one would like to have both force and displacement information along all three axes, but this is not yet possible. In addition, the capabilities of the microscope have not yet been fully exploited. For example, much of the work to date has been done at relatively low resolution during the experiments, with more detailed analysis done afterward (but without the need to remove the sample from the microscope). One can certainly extend this approach to use more of the capabilities of the microscope; for instance, electron energy-loss spectroscopy has been successfully applied to monitor tribochemical reactions such as the formation of graphitic material during sliding on diamondlike carbon.[55]

Is it possible to extend this approach down to the atomic scale, perhaps to watch while a single dislocation near the surface is pushed by a tip? Maybe. Certainly, there are technical challenges in terms of not only managing extremely small and slow (angstroms per second) displacements and simultaneously achieving sufficient stability within the microscope but also obtaining sufficient brightness to perform the imaging. However, because of the recent advent of aberration-free microscopy, it has become possible to achieve directly interpretable high-resolution images with little to no contrast reversals and much improved signal-to-noise ratios. With computer control of advanced aberration-correcting lenses, the traditional limitations on microscope performance due to spherical and chromatic aberration are removed, thereby improving spatial resolution, contrast, sensitivity, and flexibility of design for electron optical instruments.[56] Traditionally, the space between the two poles of the objective lens where a TEM sample resides has a narrow gap in high-resolution instruments, because this helps to minimize spherical aberration. However, with the ability to correct these aberrations, the size of the gap (and the space available for *in situ* instrumentation) increases. Correctin1g for spherical aberration also has the major benefit of limiting (or eliminating) contrast reversals in high-resolution images without processing schemes such as through-focal series reconstruction. This is particularly important for *in situ* experiments, as practical dynamic imaging requires that only one focal setting can be used for an experiment.

Even without these advances, there is plenty to see at the no-longer-hidden tribological interface and plenty of reason to anticipate even more dramatic results from *in situ* studies in the future.

References

1. G. Binnig, C.F. Quate, C. Gerber, *Phys. Rev. Lett*. **56**, 930 (1986).
2. C.M. Mate, G.M. McClelland, R. Erlandsson, S. Chiang, *Phys. Rev. Lett*. **59**, 1942 (1987).
3. J. Krim, D.H. Solina, R. Chiarello, *Phys. Rev. Lett*. **66**, 181 (1991).
4. E.T. Watts, J. Krim, A. Widom, *Phys. Rev. B* **41**, 3466 (1990).
5. D. Tabor, Rh. Winterto, *Proc. R. Soc. London, Ser. A* **312**, 435 (1969).
6. T.W. Scharf, I.L. Singer, *Tribol. Lett*. **14**, 3 (2003).
7. N.T. McDevitt, M.S. Donley, J.S. Zabinski, *Wear* **166**, 65 (1993).
8. P.M. Cann, H.A. Spikes, *Tribol. Trans*. **34**, 248 (1991).
9. T.W. Scharf, I.L. Singer, *Tribol. Lett*. **14**, 137 (2003).
10. M. Jean-Michel, L. Hong, M. Thiery Le, M. Maryline, *Tribol. Lett*. **14**, 25 (2003).
11. J. de la Figuera, K. Pohl, O.R. de la Fuente, A.K. Schmid, N.C. Bartelt, C.B. Carter, R.Q. Hwang, *Phys. Rev. Lett*. **86**, 3819 (2001).
12. N. Gane, *Proc. R. Soc. London, Ser. A* **317**, 367 (1970).
13. N. Gane, F.P. Bowden, *J. Appl. Phys*. **39**, 1432 (1968).
14. M. Kuwabara, W. Lo, J.C.H. Spence, *J. Vac. Sci. Technol. A* **7**, 2745 (1989).
15. W.K. Lo, J.C.H. Spence, *Ultramicroscopy* **48**, 433 (1993).
16. J.C.H. Spence, W. Lo, M. Kuwabara, *Ultramicroscopy* **33**, 69 (1990).
17. J.C.H. Spence, *Ultramicroscopy* **25**, 165 (1988).
18. M.I. Lutwyche, Y. Wada, *Sens. Actuators A* **48**, 127 (1995).
19. M.I. Lutwyche, Y. Wada, *Appl. Phys. Lett*. **66**, 2807 (1995).
20. Y. Naitoh, K. Takayanagi, M. Tomitori, *Surf. Sci*. **357**, 208 (1996).
21. T. Kizuka, N. Tanaka, S. Deguchi, M. Naruse, *Microsc. Microanal*. **4**, 218 (1998).
22. T. Kizuka, K. Yamada, S. Deguchi, M. Naruse, N. Tanaka, *J. Electron Microsc*. **46**, 151 (1997).
23. T. Kizuka, K. Yamada, S. Deguchi, M. Naruse, N. Tanaka, *Phys. Rev. B* **55**, R7398 (1997).
24. H. Ohnishi, Y. Kondo, K. Takayanagi, *Nature* **395**, 780 (1998).
25. H. Ohnishi, Y. Kondo, K. Takayanagi, *Surf. Sci*. **415**, L1061 (1998).

26. K. Svensson, Y. Jompol, H. Olin, E. Olsson, *Rev. Sci. Instrum*. **74**, 4945 (2003).
27. D. Erts, A. Lõhmus, R. Lõhmus, H. Olin, *Appl. Phys. A* **72(Suppl.)**, S71 (2001).
28. D. Erts, A. Lõhmus, R. Lõhmus, H. Olin, A.V. Pokropivny, L. Ryen, K. Svensson, *Appl. Surf. Sci*. **188**, 460 (2002).
29. T. Kizuka, H. Ohmi, T. Sumi, K. Kumazawa, S. Deguchi, M. Naruse, S. Fujisawa, S. Sasaki, A. Yabe, Y. Enomoto, *Jpn. J. Appl. Phys*. **40**, L170 (2001).
30. T. Kuzumaki, Y. Mitsuda, *Jpn. J. Appl. Phys*. **45**, 364 (2006).
31. M. Nakajima, F. Arai, T. Fukuda, *IEEE Trans. Nanotechnol*. **5**, 243 (2006).
32. A. Nafari, D. Karlen, C. Rusu, K. Svensson, H. Olin, P. Enoksson, *Proceedings of the 20th IEEE International Conference on Micro Electro Mechanical Systems (MEMS 2007)*, January 21–25, 2007, Kobe, Japan, pp. 103–106.
33. A.M. Minor, J.W. Morris, Jr., E.A. Stach, *Appl. Phys. Lett*. **79**, 1625 (2001).
34. M.S. Bobji, J.B. Pethica, B.J. Inkson, *J. Mater. Res*. **20**, 2726 (2005).
35. M.S. Bobji, C.S. Ramanujan, J.B. Pethica, B.J. Inkson, *Meas. Sci. Technol*. **17**, 1324 (2006).
36. A. Nafari, A. Danilov, H. Rödjegärd, P. Enoksson, H. Olin, *Sens. Actuators A* **123–124**, 44 (2005).
37. K.A. Rzepiejewska-Malyska, G. Buerki, J. Michler, R.C. Major, E. Cyrankowski, S.A. Syed Asif, O.L. Warren, *J. Mater. Res*. **23**, 1973 (2008).
38. A. Merkle, L.D. Marks, *Wear* **265**, 1864–1869 (2008).
39. A.P. Merkle, L.D. Marks, *Appl. Phys. Lett*. **90**, 064101 (2007).
40. M. Dienwiebel, N. Pradeep, G.S. Verhoeven, H.W. Zandbergen, J.W.M. Frenken, *Surf. Sci*. **576**, 197 (2005).
41. M. Dienwiebel, G.S. Verhoeven, N. Pradeep, J.W.M. Frenken, J.A. Heimberg, H.W. Zandbergen, *Phys. Rev. Lett*. **92**, 126101 (2004).
42. A.P. Merkle, L.D. Marks, *Tribol. Lett*. **26**, 73 (2007).
43. A.P. Merkle, L.D. Marks, *Philos. Mag. Lett*. **87**, 527 (2007).
44. E.A. Stach, T. Freeman, A.M. Minor, D.K. Owen, J. Cumings, M.A. Wall, T. Chraska, R. Hull, J.W. Morris, Jr., A. Zettl, U. Dahmen, *Microsc. Microanal*. **7**, 507 (2001).
45. A.M. Minor, S.A. Syed Asif, Z.W. Shan, E.A. Stach, E. Cyrankowski, T.J. Wyrobek, O.L. Warren, *Nat. Mater*. **5**, 697 (2006).
46. W.A. Soer, J.Th.M. De Hosson, A.M. Minor, Z.W. Shan, S.A. Syed Asif, O.L. Warren, *Appl. Phys. Lett*. **90**, 181924 (2007).
47. O.L. Warren, Z.W. Shan, S.A. Syed Asif, E.A. Stach, J.W. Morris, Jr., A.M. Minor, *Mater. Today* **10(4)**, 59 (2007).
48. A. Gouldstone, N. Chollacoop, M. Dao, J. Li, A.M. Minor, Y.L. Shen, *Acta Mater*. **55**, 4015 (2007).
49. Y. Sun, J. Ye, Z.W. Shan, A.M. Minor, T.J. Bulk, *JOM* **59(9)**, 54 (2007).
50. K.J. Hemker, W.D. Nix, *Nat. Mater*. **7**, 97 (2008).
51. Z.W. Shan, R.K. Mishra, S.A. Syed Asif, O.L. Warren, A.M. Minor, *Nat. Mater*. **7**, 115 (2008).
52. Z.W. Shan, J. Li, Y.Q. Cheng, A.M. Minor, S.A. Syed Asif, O.L. Warren, E. Ma, *Phys. Rev. B* **77**, 155419 (2008).
53. Z.W. Shan, G. Adesso, A. Cabot, M.P. Sherburne, S.A. Syed Asif, O.L. Warren, D.C. Chrzan, A.M. Minor, A.P. Alivisatos, *Nat. Mater*. (2008), in press.
54. C.A. Schuh, *Mater. Today* **9(5)**, 32 (2006).
55. A. Merkle, L.D. Marks, O. Eryilmaz, A. Erdimer, manuscript in preparation.
56. C. Kisielowski, B. Freitag, M. Bischoff, H. van Lin, S. Lazar, G. Knipels, P. Tiemeijer, M. van der Stam, S. von Harrach, M. Stekelenburg, M. Haider, S. Uhlemann, H. Muller, P. Hartel, B. Kabius, D. Miller, I. Petrov, E.A. Olson, T. Donchev, E.A. Kenik, A.R. Lupini, J. Bentley, S.J. Pennycook, I.M. Anderson, A.M. Minor, A.K. Schmid, T. Duden, V. Radmilovic, Q.M. Ramasse, M. Watanabe, R. Erni, E.A. Stach, P. Denes, U. Dahmen, *Microscopy and Microanalysis* **14**, 469–477 (2008). □